Int. J. Electrochem. Sci., 7 **(2012)** 11297 - 11312

International Journal of
ELECTROCHEMICAL
SCIENCE
www.electrochemsci.org

Effects Of Sulfate-Reducing Bacteria on Corrosion of Carbon Steel Q235 in the Crevice by EIS

Jin Xu[*], *Cheng Sun, Maocheng Yan, Fuhui Wang*

State Key Laboratory for Corrosion and Protection, Institute of Metals Research, Chinese Academy of Sciences, Shenyang 110016, China
[*]E-mail: xujin@imr.ac.cn

Received: 25 September 2012 / *Accepted:* 16 October 2012 / *Published:* 1 November 2012

The effect of sulfate reducing bacteria (SRB) on the corrosion of the carbon steel Q235 was investigated in the crevice under the simulated disbonded coating in the soil-extract solutions (SES). The results of electrochemical impedance spectroscopy (EIS) showed that the active biofilm enhanced the corrosion of the carbon steel in SES with SRB. The comparison of polarization (R_p) and charge transfer resistances (R_t) indicated that biofilm seriously influenced the reaction of the metal/solution interface and the corrosion rate of the carbon steel. The results of scanning electron microscopy (SEM) and energy disperse X-ray analysis (EDXA) found that the metabolic sulfide preferred forming on the surface of the soil grains to on the others. SRB was observed on the surface of the corrosion products.

Keywords: SRB; simulated disbonded coating; EIS; metabolic sulfide

1. INTRODUCTION

Highly insulating coatings and the cathodic protection are widely used to protect buried steel pipelines from external corrosion. However, corrosion of the steel will occur once a crevice between the coating and the pipeline is formed.

Many researches[1-13] have been investigated about the corrosion of the metal in the crevice under the disbonded coatings since nineteen seventies. Peterson and Lennox[1] have concluded that the cathodic protection can be achieved in the crevices even though the ratio of the distance to crevice opening is 12000:1. Some researchers[2, 3, 5, 6] have indicated that the steel can be protected in the crevice if only enough protective potentials are applied at the holiday. Beavers and Thompson[4] have showed that PET coatings can shield CP current while coal tar and FBE coatings do not. Perdomo et al.[9-10] have studied the effects of chemical and electrochemical conditions on the steel under the disbonded coatings. The results show that the effective cathodic protection results in the consumption

of oxygen in the water and the increase in alkalinity. Corrosion protection is achieved in the "shielded" area by the chemical modification. Chemical changes affecting the potential in previously oxidized surfaces occur more slowly than those observed in bare steel conditions.

The above studies mainly focus on the effects of abiotic factors on the metals or the corrosion of the metals in the crevices under disbonded coatings, but the effects of biotic factors, e.g., sulfate reducing bacteria (SRB), are seldom investigated. In our prior study, microbiological influenced corrosion of the carbon steel has been investigated in the crevice with 0.5 mm in thickness[14]. The results show that SRB has a important effect on the corrosion of the steel in the crevice.

In this paper, the effects of SRB on the corrosion of carbon steel Q235 are further investigated in the crevices, the thickness of which is 1.0 mm, by using electrochemical impedance spectroscopy (EIS), scanning electron microscopy (SEM), and energy dispersive x-ray analysis (EDXA).

2. EXPERIMENTAL

2.1. Crevice cell

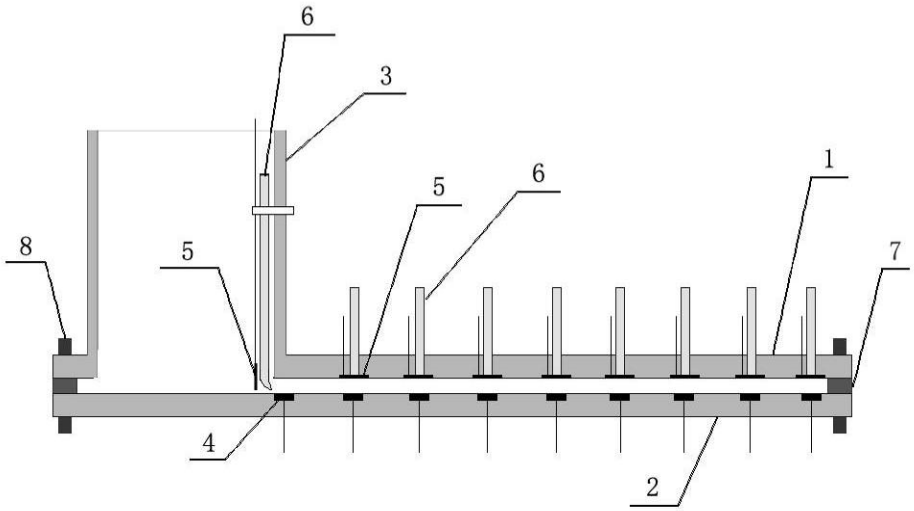

(a) Side view

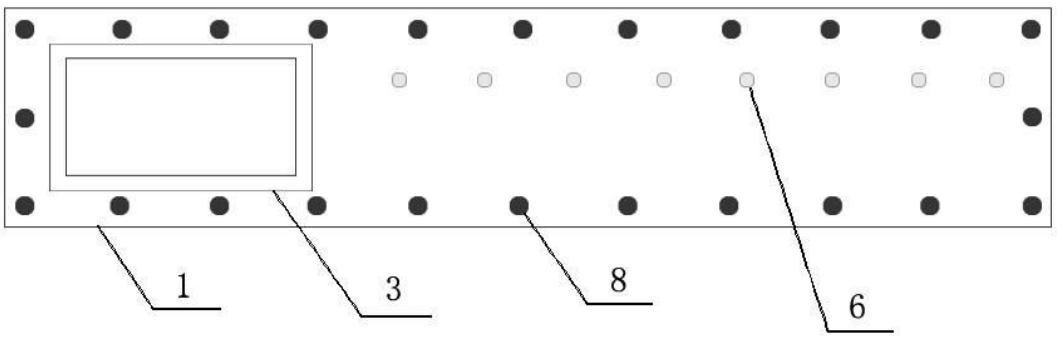

(b) Top view

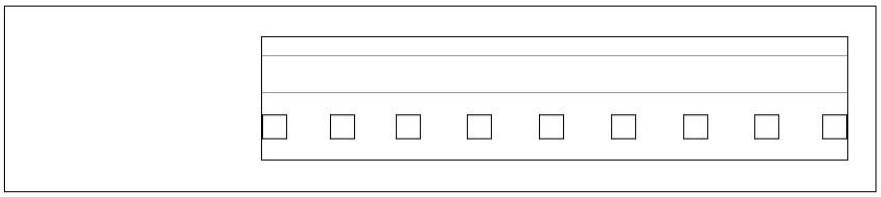

(c) Working electrode

Figure 1. Schematic diagram of the electrochemical cell simulating a crevice (1: top plate; 2: bottom plate; 3: container; 4: working electrode; 5: counter electrode; 6: salt bridge; 7: PTFE gasket; 8: bolt)

All the experiments were performed using an electrochemical cell[14], as shown in Fig. 1. This cell was designed to simulate the crevice normally found between the disbonded coating and the buried pipeline steel. A rectangular crevice 500 mm length and 100 mm width was formed by bolting a polytetrafluoroethylene (PTFE) gasket (thickness was 1.0 mm in this research) between two polymethylmethacrylate (PMMA) plates. The thickness of the PTFE gasket was chosen to control the crevice thickness. A cuboid (150 mm in the length, 100 mm in the width, and 200 mm in the height) was adhered to the top plate to serve as the bulk solution container. Nine carbon steel Q235 electrodes and eight electrodes of stainless steel 316 were sealed in the top and the bottom plate along the crevice length, and served as working electrodes and counter electrodes, respectively. Eight salt bridges filled with the soil-extract solution (SES) were installed in order to measure the EIS, and the distances from the holiday were 70, 130, 190, 250, 310, 370, 430 and 490 mm.

2.2. Coupon preparation

Samples of nine small coupons of carbon steels (20×20×3mm) and one big coupon (30×500×3mm), which served as working electrodes, as shown in Fig. 1(c), were cut from a plate of the carbon steel Q235 with the nominal composition (wt %) of 0.30C, 0.019P, 0.029S, 0.01Si, 0.42Mn, and balance Fe.

Samples of 30×30×2mm, which served as counter electrodes, were cut from a plate of the stainless steel 316 with the nominal composition (wt %) of 17.82Cr, 12.93Ni, 2.19Mo, 0.06C, 0.037P, 0.029%S, 0.35Si, 1.69Mn, and balance Fe.

The coupons were abraded with a series of grit papers (200, 400, 600, 800) followed by cleaning in the acetone and the alcohol and dried. Both the working and the counter electrodes were sterilized under the ultraviolet rays prior to the experiment.

2.3. Soil solution preparation

Soils used in this study were taken from Shenyang soil experimental station, China. The soil-extract solution (SES) was prepared by extracting the soil solution with the water-soil ratio of 5:1. The

compositions of the SES are given in table 1. The SES was autoclaved at 121℃ for 20 min and stored at 4℃ before use.

Table 1. Compositions of the SES (mg/L)

pH	Chemical composition						Organic content	Whole nitrogen content	Total salt content
	Cl^-	SO_4^{2-}	Ca^{2+}	Mg^{2+}	K^+	Na^+			
7.41	9.8	50.6	27.2	10.2	2.4	9.8	7240	364	200

2.4. Microorganisms

Sulfate reducing bacteria stains[15] used in this study was isolated from soils taken from Shenyang soil experimental station in order to investigate MIC of the carbon steel Q235 in soil environments. They were anaerobically incubated in the API RP-38 medium (g/L)[16] containing $MgSO_4 \cdot 7H_2O$ 0.2; ascorbic acid 1.0, NaCl 10.0, KH_2PO_4 0.5, Sodium lactate 4.0, Yeast extract 1.0, $Fe(NH_4)_2(SO_4)_2$ 0.02, for enrichment, and was subsequently purified in sterile agar plates using the API RP-38 medium by picking up several single black colonies with a sterile inoculation loop.

Twenty milliliters of the culture were subsequently transferred into the individual 1000 mL of the sterilized SES. After 2 days incubation, the inoculated SES was added in the testing devices for the corrosion experiments

2.5. EIS analysis

The electrochemical impedance spectroscopy was used to investigate the electrochemical properties of the corroded surface after the immersion in the SES over time. All experiments were performed in a three-electrode electrochemical cell, with the stainless steel electrode used as the counter electrode, and the saturated calomel electrode (SCE) as the reference electrode. The test was operated using the PARSTAT 2273 electrochemical measurement system manufactured by the EG&G. The frequency range was from 1 mHz to 100 kHz and the amplitude of the sinusoidal voltage signal was 10 mV. The EIS data obtained were modeled and simulated using the Zsimpwin software supplied by the PARSTAT2273.

2.6. SEM and EDS analysis

In the SEM study, the surface appearance of the carbon steel Q235 in the SES was visualized after a preparation using the following procedure. Samples were fixed with the 3 vol% glutaraldehyde in a phosphate buffer solution (PBS, pH 7.3–7.4) for more than 4 h, and then washed with the PBS for two changes (5 min each), rinsed with the distilled water for another two changes (5 min each), and dehydrated with using an ethanol gradient (at 50%, 75%, 95% and 99% for 10 min) before being

finally stored in a desiccator. A scanning electron microscope (XL30-FEG) with the beam voltage at 25 kV was used to visualize the morphology of surface.

3. RESULTS AND DISCUSSIONS

3.1. Variation of SRB numbers and pH values

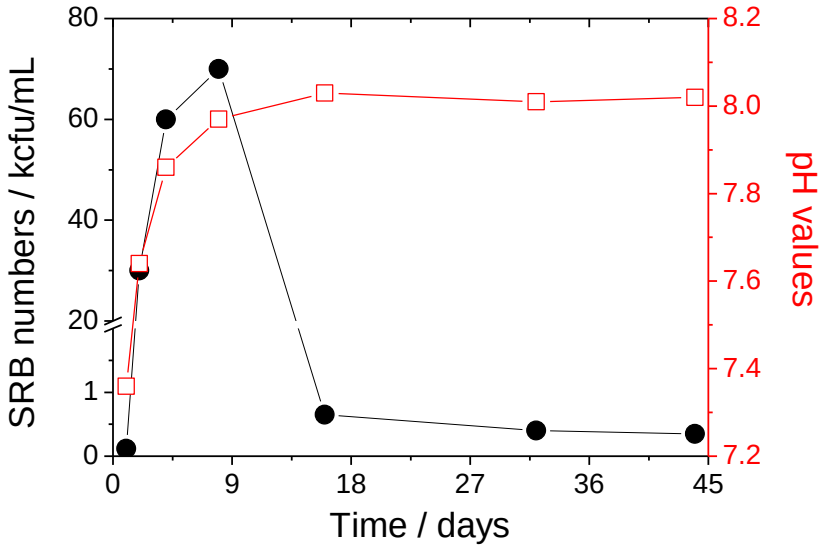

Figure 2. Variation of SRB numbers and pH values with time in the SES

Figure 2 shows the variations of the SRB numbers and the pH values with time in the SES. The SRB numbers sharply increased to 70000 cfu/mL ("cfu" is an abbreviation of "colony forming unit") by the end of eighth day, rapidly decreased to 650 cfu/mL after 16 days, and then remained stable. The pH increased with time, reaching a peak after 16 days , and then remained stable.

During the metabolic process of the SRB, the following reaction occurs:

$$4Fe + SO_4^{2-} + 4H_2O \rightarrow FeS + 3Fe(OH)_2 + OH^-$$

The above equation indicates that the result of the whole reaction will lead to the increasing of pH value in the solutions, the increasing amplitude increases with SRB numbers increasing. The above results lead to the dramatic increasing of the pH values during the growing period of SRB. The pH values slowly increase during the early days of the dying period of SRB because there are still a large number of SRB. In the later stage of the dying period, nutrients that are limited in the SES are rather depleted during the metabolism of SRB, which results in the rapid decreasing of the SRB numbers. The amounts of metabolites sharply decrease with the SRB numbers decreasing, which leads to the

sharply decreasing of the concentrations of OH- ion newly formed. The above results are the reasons of little change of pH value of the SES.

3.2. Potential distributions

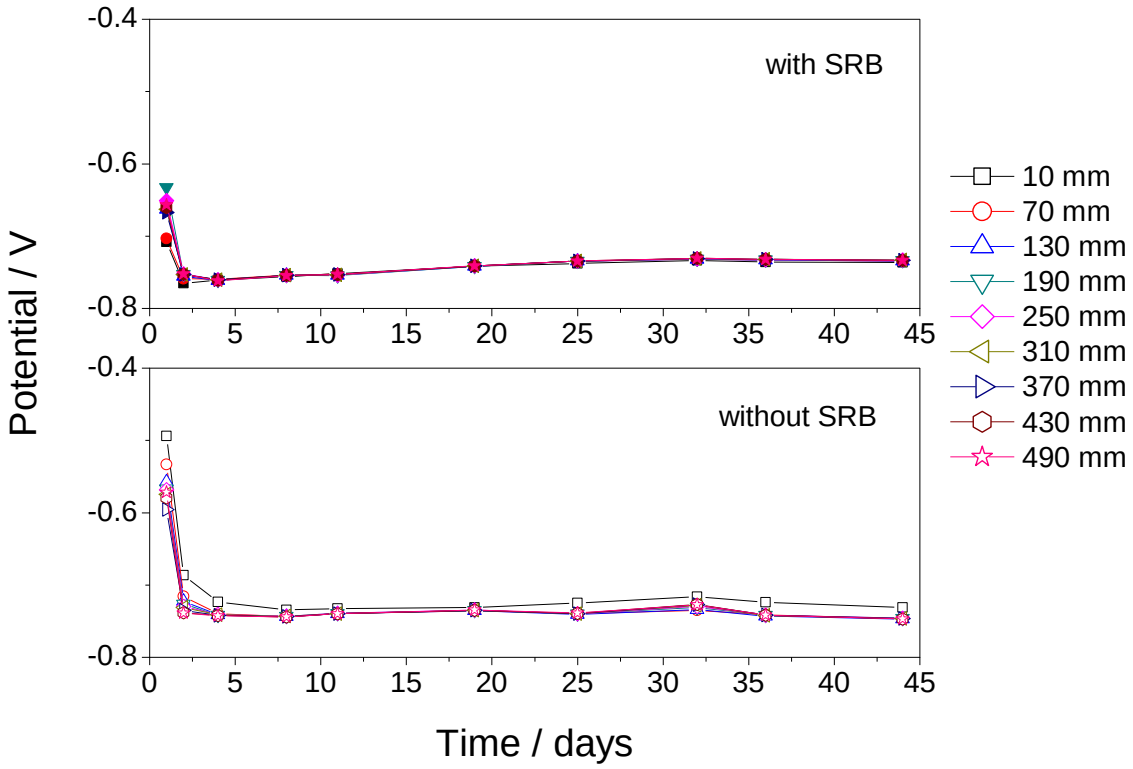

Figure 3. Local potentials with the distance and the time under the disbonded coatings in the SES

Figure 3 shows the potential distributions with time under the simulated disbonded coatings in the SES. The potentials dramatically decrease in the SES without SRB, and remain stable. The potential decrease is mainly due to the dissolution of the natural oxide film in the SES without SRB[17-19]. At the same time, newly corrosion products are formed on the surface of the steel with experiment going. When the thickness of the corrosion film achieves a dynamic stable value, the potentials keep relatively stable.

The potentials dramatically decrease in the SES with SRB, slowly increase, and then remain stable. There are two reasons leading to the decreasing of the potentials: one reason is that the dissolution of the oxide films naturally formed. The other is that the biofilms containing bacteria and extracellular ploymetric substance (EPS), which are negatively charged[20-21]. The above results will make the potentials of the metal surfaces decrease. When the bacteria die away with time, the negative charges of the surface gradually decrease, which leads to the potential increase. At the same time, new oxide films or corrosion product films formed on the surface of the steel also increase the potential.

This result is similar to that of Moon's conclusion regarding corrosion potential variations[22].

3.3. EIS analysis

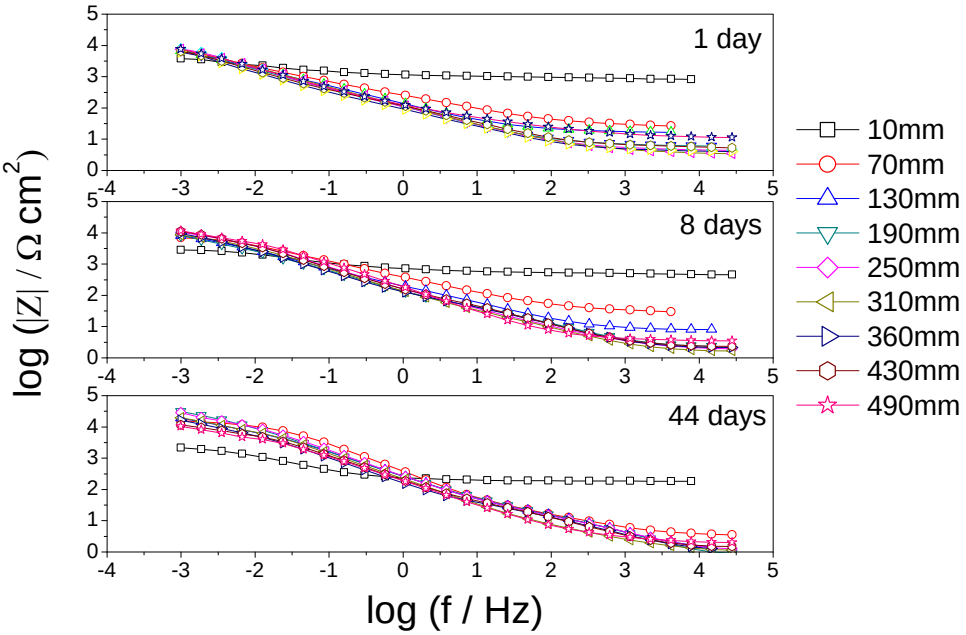

(a) Modulus vs frequency

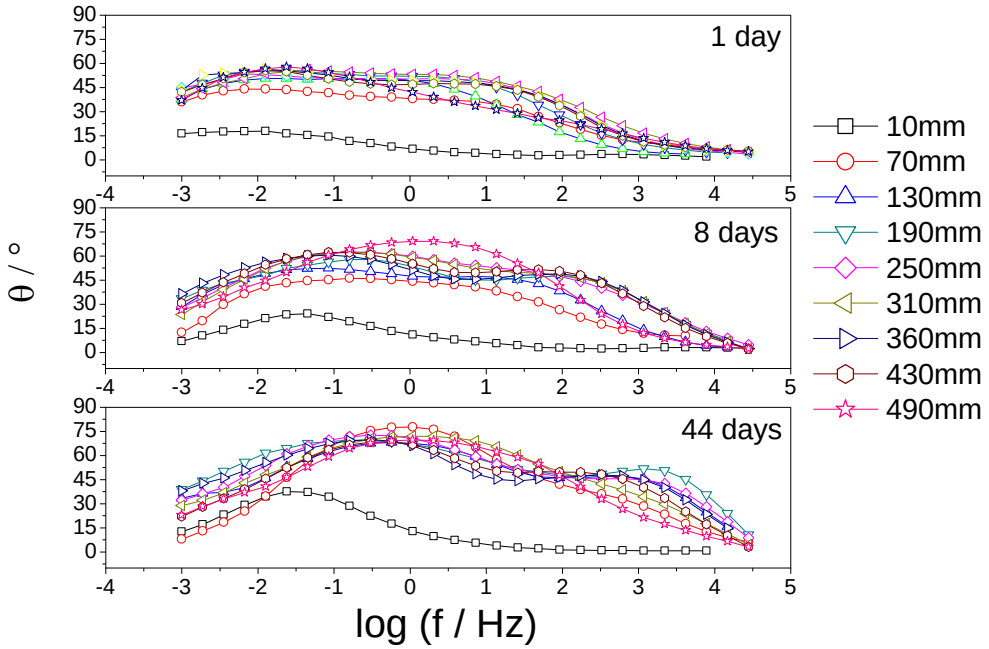

(b) Phase angle vs frequency

Figure 4. Bode plots of the carbon steel Q235 with time in the SES with SRB

Figure 4 and 5 show the Bode plots of the carbon steel Q235 with distance in the SES with and without SRB after immersing for 1 day, 8 days and 44 days, and the equivalent circuits are given in

Fig. 6. R_s represents an electrolyte resistance, R_f and Q_f represent a resistance and a capacitance of the film of the corrosion products, R_{bio} and Q_{bio} represent a resistance and a capacitance of the biofilms, R_t and Q_{dl} represent a charge transfer resistance and a double layer capacitance, respectively. The fitting results are listed in Table 2, 3 and 4.

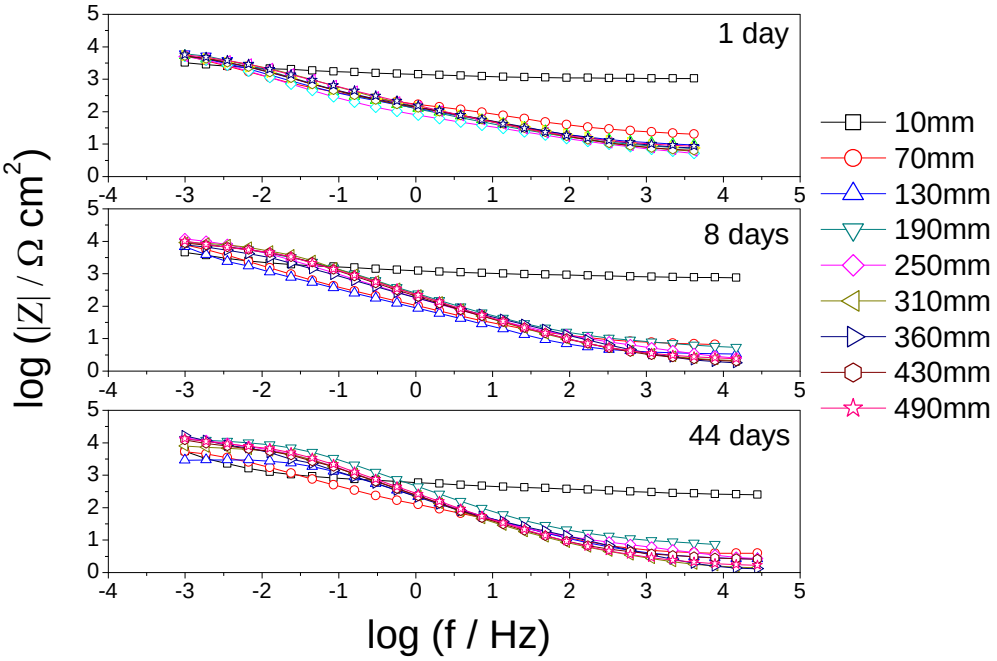

(a) Modulus vs frequency

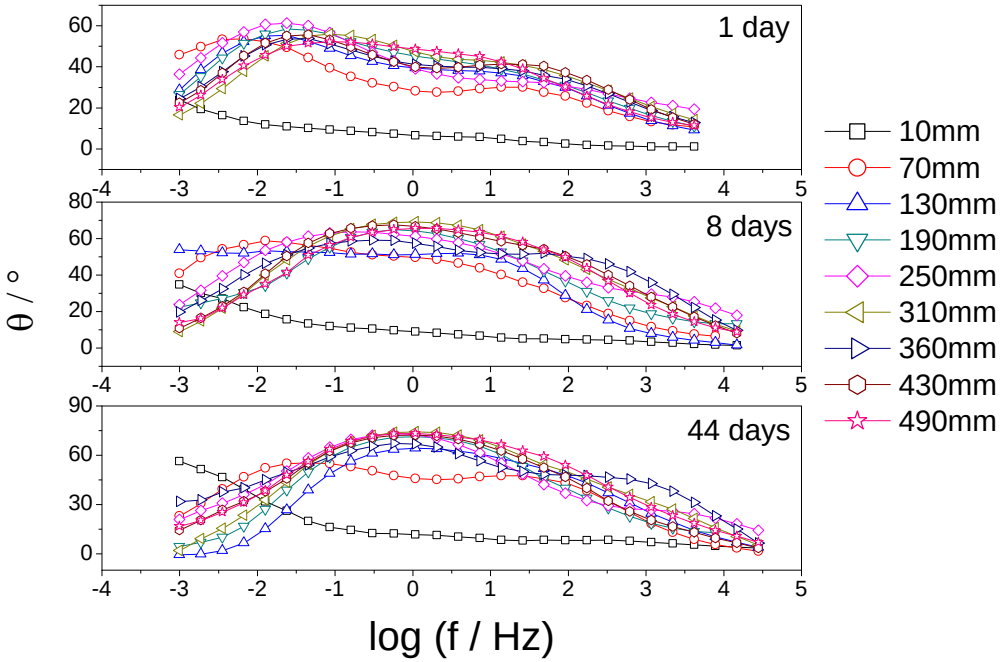

(b) Phase angle vs frequency

Figure 5. Bode plots of the carbon steel Q235 with time in the SES without SRB

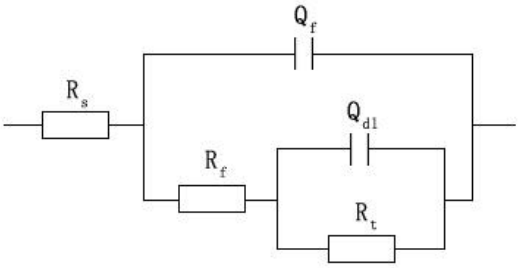

(a) Two time constants

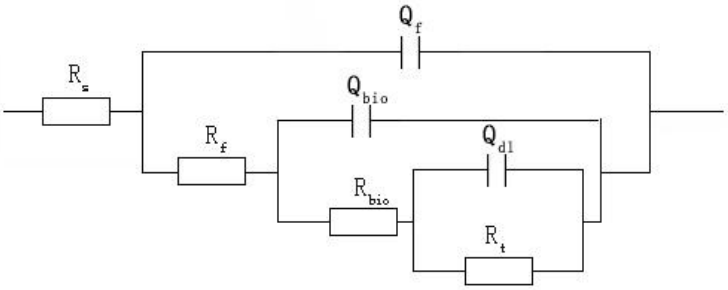

(b) Three time constants

Figure 6. Equivalent circuits of the different time constants

Table 2. Fitting results of EIS in the SES after 1 day

Distance mm	R_s Ω cm^2	R_f Ω cm^2	Y_f mS sec^n/ cm^2	n_f	R_t kΩ cm^2	Y_{dl} mS sec^n/cm^2	n_t
With SRB							
10	779.9	231	0.06588	0.5133	5.529	1.950	0.4619
70	25.84	908.9	1.226	0.5551	20.06	1.201	0.6519
130	16.59	3861	2.410	0.6246	12.72	1.554	0.8888
190	6.156	1757	2.789	0.6387	20.08	1.024	0.9026
250	4.454	838.7	2.541	0.6418	24.75	0.9963	0.8932
310	3.499	1826	2.560	0.6263	19.36	0.4143	1
370	4.029	541.6	3.034	0.6339	19.02	1.866	0.8432
430	5.437	619.1	2.367	0.6258	17.72	1.982	0.8398
490	11.38	73.83	1.149	0.6062	21.07	1.952	0.704
Without SRB							
10	962.2	1514	0.6578	0.4073	11.48	6.507	0.6257
70	17.61	313.1	1.404	0.5163	34.03	3.611	0.7593
130	8.617	308	1.893	0.5789	10.90	2.329	0.8487
190	6.572	149	1.597	0.6136	11.35	1.487	0.7907
250	3.467	69.05	1.873	0.5569	16.91	3.226	0.8039
310	4.933	161.6	1.410	0.6069	6.543	0.8909	0.8288
370	6.093	310.8	1.725	0.5673	9.007	1.476	0.8605
430	5.284	273.5	1.584	0.5945	7.589	1.872	0.8728
490	8.274	224.8	1.560	0.6173	8.050	0.6390	0.7199

Table 3. Fitting results of EIS in the SES after 8 days

Distance mm	R_s Ω cm^2	R_f Ω cm^2	Y_f mS sec^n/ cm^2	n_f	R_{bio} kΩ cm^2	Y_{bio} mS sec^n/ cm^2	n_{bio}	R_t kΩ cm^2	Y_{dl} mS sec^n/cm^2	n_t
With SRB										
10	366.6	189.8	0.09057	0.4254	-	-	-	4.240	1.964	0.5714
70	13.99	531.5	0.7570	0.619	-	-	-	28.70	0.3645	0.6288
130	3.124	95.43	1.103	0.6622	8.58	0.8934	0.6734	5.653	16.84	1
190	1.28	59.74	0.8929	0.6959	8.592	0.7887	0.8045	14.82	6.662	0.8708
250	1.596	38.24	0.9336	0.7066	11.33	0.5814	0.78	7.300	16.62	1
310	1.404	42.9	1.079	0.7201	7.218	0.5316	0.8557	7.981	9.848	0.9519
370	1.465	90.61	0.9311	0.6909	9.804	1.048	0.8259	14.74	7.383	0.9101
430	1.899	132.6	0.8932	0.705	8.019	0.6037	0.8684	11.49	8.383	0.8885
490	3.123	4.699	0.4410	0.8071	4.943	0.6364	0.8061	11.79	6.017	0.8224
Without SRB										
10	521.1	3285	1.119	0.1925	-	-	-	1.321E+04	11.02	0.7221
70	3.997	1173	1.758	0.6472	-	-	-	9.789E+03	0.2868	0.9396
130	2.321	305.3	1.155	0.6907	-	-	-	7.558E+03	0.1865	0.8213
190	4.655	19.05	0.3547	0.768	-	-	-	1.246E+04	0.3482	0.8224
250	2.012	10.94	0.3398	0.7235	-	-	-	1.121E+04	0.9009	0.7765
310	1.723	9.751	0.3759	0.8045	-	-	-	1.070E+04	0.4887	0.8346
370	1.305	138.9	1.040	0.6757	-	-	-	1.344E+04	0.2426	0.919
430	1.721	39.96	0.7605	0.778	-	-	-	1.217E+04	0.2757	0.8425
490	2.126	7.169	0.3081	0.8074	-	-	-	2.091E+04	0.3607	0.8005

Table 4. Fitting results of EIS in the SES after 44 days

Distance mm	R_s Ω·cm^2	R_f Ω·cm^2	Y_f mS·sec^n/ cm^2	n_f	R_{bio} kΩ·cm^2	Y_{bio} mS·sec^n/ cm^2	n_{bio}	R_t kΩ·cm^2	Y_{dl} mS·sec^n/cm^2	n_t
With SRB										
10	187.5	-	-	-	-	-	-	2.389	4.390	0.6634
70	3.571	28.57	0.2966	0.7775	-	-	-	15.45	0.2320	0.9578
130	1.196	31.56	0.4278	0.7353	-	-	-	14.26	0.4674	0.8168
190	0.8022	19.26	0.1955	0.8141	-	-	-	52.73	0.6981	0.757
250	1.134	26.4	0.3452	0.7562	-	-	-	27.01	0.4702	0.8352
310	1.106	14.84	0.8366	0.7359	-	-	-	22.76	0.1985	0.977
370	0.9772	70.57	0.9727	0.6672	-	-	-	29.70	0.4619	0.9844
430	1.318	94.7	0.9081	0.6919	-	-	-	13.72	0.2750	0.9991
490	1.976	3.666	0.4606	0.801	6.786	0.7525	0.7839	5.675	14.06	1
Without SRB										
10	17.3	3523	1.526E-03	0.1821	-	-	-	22.97	17.94	0.8723
70	3.728	192.6	1.386E-03	0.6744	-	-	-	7.275	1.853	0.7541
130	2.788	29.51	0.5655	0.7749	-	-	-	3.171	0.4178	0.7997
190	7.833	21.54	0.1945	0.8251	-	-	-	11.42	0.2626	0.8362
250	2.431	10.71	0.2716	0.7272	-	-	-	11.96	0.6115	0.8417
310	1.404	8.173	0.3742	0.8158	-	-	-	7.684	0.4918	0.858
370	1.122	71.38	0.9089	0.6753	-	-	-	17.76	0.2111	0.9782
430	2.62	5.672	0.3537	0.8144	-	-	-	9.012	0.5531	0.8135
490	1.652	5.145	0.3182	0.8212	-	-	-	10.92	0.4539	0.8204

There were two time constants in the SES after immersing for 1 day. The time constant at the high frequency for the SES with SRB might be due to the forming of composite films containing corrosion product films and biofilm. Biofilm was not formed on the surface of the steel because SRB was in an adaptive period for a new environment. The time constant for the SES without SRB might be due to the forming of corrosion product films. The second time constant at the lowest frequency appeared because the protective ability of the film was not perfect.

The spectra obtained in the SES with SRB after immersing for 8 days had two time constants at distances of 10 mm and 70 mm from the holiday, and three time constants at other distances. The time constant at the high frequency might be due to the forming of the corrosion product films; the time constant at the middle frequency might be due to the forming of biofilm by SRB in the crevices, but the time constant of the middle frequency was not formed because the oxygen concentrations at the positions close to the holiday were much more in the SES than that in the crevice, which inhibited the growth of SRB and forming of biofilm; the third time constant at the lowest frequency appeared because the protective ability of the film of the corrosion products and biofilm was not perfect. Two time constants were also observed in the SES without SRB after 8 days.

Except for those at the distance of 10 mm and 490mm, there are two time constants in the SES with SRB after 44 days, which is due to the death of SRB and the destroying of the biofilm, and a composite film containing the destroyed biofilm and the corrosion product films is formed.

There is only one time constant at the distance of 10 mm from the holiday in the SES with SRB after 44 days, which is due to the abscission of the corrosion product film, and three time constants are observed at the distances of 490 mm, which indicates that the biofilm here is still active. There are two time constants at other distances for the death of SRB and the destroying of the biofilms, which shows that the biofilms have lost their activities and been absorbed in the corrosion product films.

The amounts of the time constants are not changed in the SES without SRB after 44 days.

The charge transfer resistance, R_t, was expressed as following relation[23]:

$$\frac{1}{R_t} = \left(\frac{\partial I_F}{\partial E} \right)_{X_i}$$

where R_t is the charge transfer resistance, I_F is the faraday current, E is the potential, and X_i is the state variable.

The comparing results of R_t values in the SES with and without SRB after immersing for different days are listed in Fig. 7.

R_t values are bigger in the SES with SRB than those without SRB for most positions in the crevice at the first day, which indicates that SRB does not accelerate the corrosion rates of the steel in the early period. The above result is due to the reason that biofilms containing SRB and extracellular polymeric substance (EPS), which are negatively charged[20-21] and repellent to corrosive anions, are formed on the surface of the steel in the presence of SRB.

The values of R_t are almost the same in the SES with and without SRB for the most positions in the crevice after 8 day. The reason is that the amounts of the metabolites, e.g., ferrous sulfide, increase

with SRB increasing, which accelerate the corrosion rates of the steel[24-28]. At the same time, the abilities of negative charge of SRB and biofilm also increase. The intensities of two effects are almost the same, which leads to the above result.

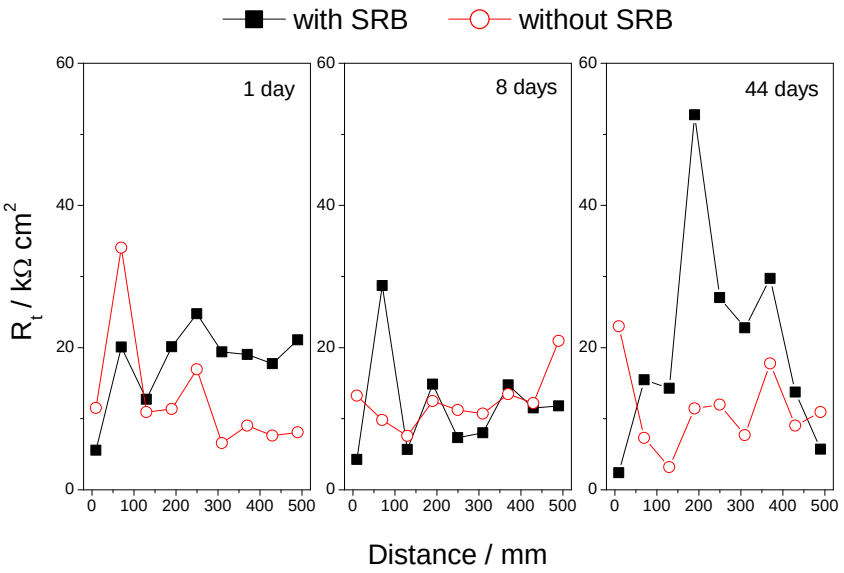

Figure 7. Comparison plot of Rt with distance in the SES with and without SRB

The values of R_t are bigger in the SES with SRB than those without SRB for the most positions in the crevice after 44 day. With the death of SRB, the amounts of the metabolites do not increase, and some corrosion products, e.g. ferrous hydroxide, accumulate inside the biofilm pores[29, 30], which enhance the protective ability of the biofilm.

The above results indicated that the activities of SRB and the biofilm formed by SRB had great influences on the reaction of the metal/solution interface of the metal and the corrosion rate of the carbon steel.

3.4. SEM and EDXA analysis

Figure 8 and 9 show scanning electron micrograph of the corrosion products on the surfaces of the carbon steel Q235 at a distance of 430 mm to the holiday under the disbonded coating in the SES with and without SRB after 44 days.

There is a composite film containing biofilm and corrosion product film on the surface of the steel in the SES with SRB, as shown in Fig. 8, and this film is compact. However, an incomplete film is observed in the SES without SRB (Fig. 9). The above results validate the EIS results. EDAX results show that there are elements C mainly from high-molecule composites, e.g., EPS, in the products for the SES with SRB, but not without SRB. The above results further indicate that the films formed on the surface of the steel are the composite films containing the biofilms and the corrosion product films.

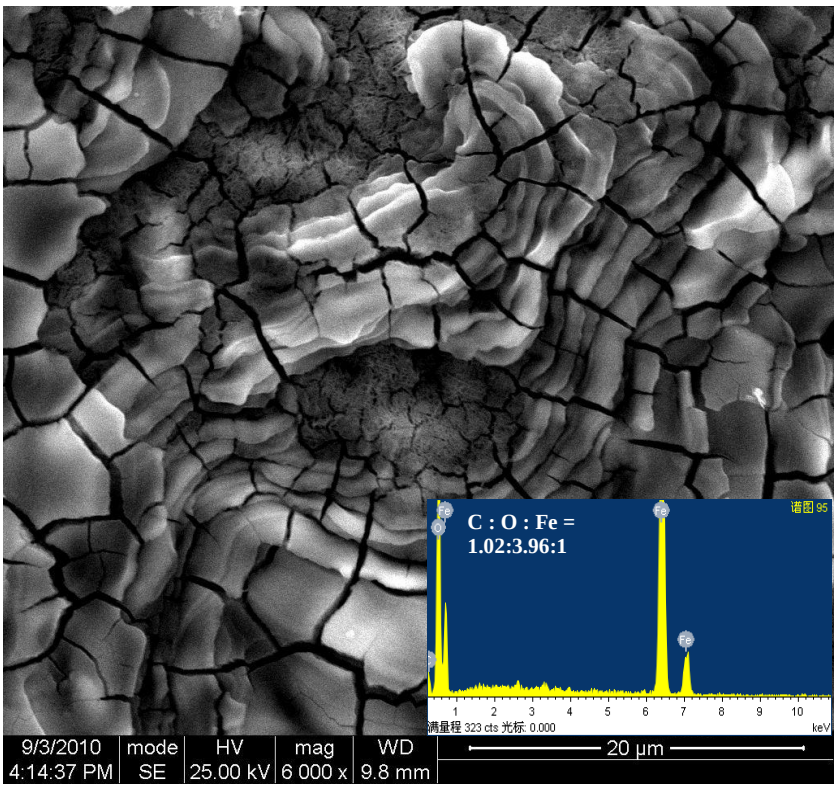

Figure 8. Scanning electron micrograph of corrosion product on the surface of the carbon steel Q235 in the SES with SRB

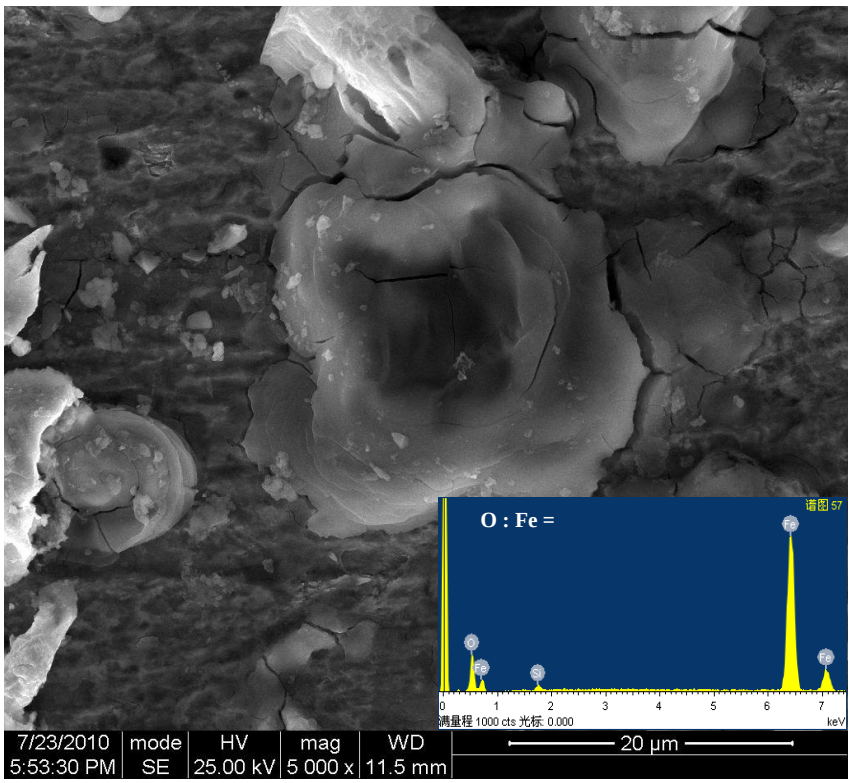

Figure 9. Scanning electron micrograph of corrosion product on the surface of the carbon steel Q235 in the SES without SRB

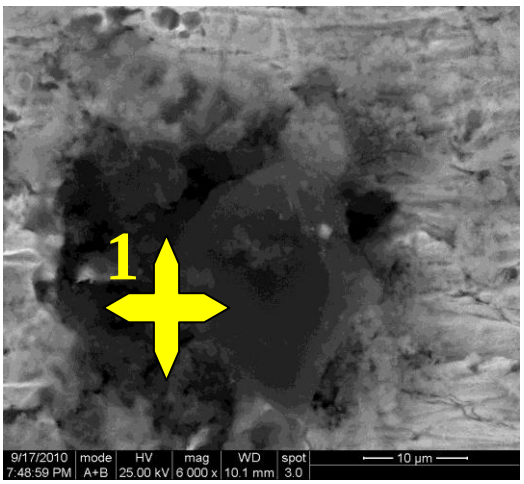

(a) 70 mm

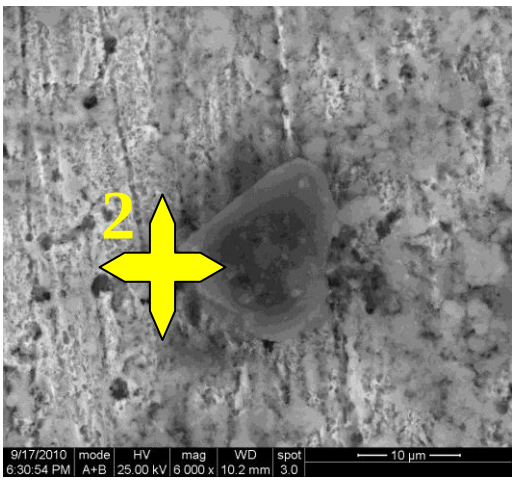

(b) 250 mm

Figure 10. Micrograph of the surface of the carbon steel Q235 in the SES with SRB at different positions

Table 5. EDXA results of products on the surface of carbon steel Q235 in the SES after immersing for 44 days

Element	Element content atom%	
	1	2
Fe	8.29	2.00
S	0.43	0.75
C	59.93	12.27
O	28.93	54.28
Al	0.43	3.49
Si	1.63	23.45
P	0.36	-
Mg	-	1.11
Ca	-	1.47
K	-	0.62
Cl	-	0.57

Three micrographs (Fig. 10) are selected to investigate the formation of metabolic sulfide, and EDXA results are listed in Table 5. Sulfur elements are observed on the surface of granular substances. Some other elements, e.g., carbon, aluminum, silicon, magnesium and calcium are also observed on the surface of these granular substances. Elements Al, Si, Mg and Ca might be mainly from tiny soil grains, and elements C are from the SRB bodies and the carbonized substances produced by SRB. The above results indicate that the metabolic sulfides prefer forming on the surface the granular substances, such as the soil grains and the carbonized substances.

4. CONCLUSIONS

4.1. Three time constants are observed in Bode plots for the carbon steel in the SES with SRB after immersing for 8 days.

4.2. The corrosion rates of the carbon steel Q235 are smaller in the SES with SRB in the most days of the experiments.

4.3. There is a compact composite film on the surface of the carbon steel in the SES with SRB, however, an incomplete film are observed for the SES without SRB.

4.4. The metabolic sulfides prefer forming on the surface of the granular substances.

ACKNOWLEDGEMENTS
The project was financially supported by the National Natural Science Foundation of China (Grant No. 51131001 and 50971128), the National R&D Infrastructure and Facility Development Program of China (Grant No. 2060503).

References

1. M.H. Peterson and T.J. Lennox JR, *Corrosion*, 29 (1973) 406.
2. R.R. Fessler, A.J. Markworth and R.N. Parkins, *Corrosion*, 39 (1983) 20.
3. F. Gan, Z.W. Sun, G. Sabde and D.T. Chin, *Corrosion*, 50 (1994) 804.
4. J.A. Beavers and N.G. Thompson, *Mater. Performance*, 4 (1997) 13.
5. P.F. Lara and E. Klechka, *Corrosion*, 6 (1999) 30.
6. A.C. Toncre and N. Ahmad, *Mater. Performance*, 6 (1980) 39.
7. R. Brousseau, S. Qian and B. Gummow, *Mater. Performance*, 6 (1993) 21.
8. R. Brousseau and S. Qian, *Corrosion*, 50 (1994) 907.
9. J.J. Perdomo and I. Song, *Corros. Sci*. 42 (2000) 1389.
10. J.J. Perdomo, M.E. Chabica and I. Song, *Corros. Sci*. 43 (2001) 515.
11. Z.F. Li, F.X. Gan and X.H. Mao, *Corros. Sci*. 44 (2002) 689.
12. X. Chen, X.G. Li, C.W. Du and Y.F. Cheng, *Corros. Sci*. 51 (2009) 2242.
13. A.Q. Fu and Y.F. Cheng, *Corros. Sci*. 52 (2010) 2511.
14. J. Xu, K. X. Wang, C. Sun, F. H. Wang, X. M. Li, J. X. Yang and C. K. Yu, *Corros. Sci*. 53 (2011) 1554.
15. C. Sun, J. Xu and F.H. Wang, *Ind. Eng. Chem. Res*, 50 (2011) 12797.
16. J. Liu , L.M. Xu and J.S. Zheng, *J. Chin. Soc. Corros. Prot.* 21 (2001) 345.
17. Y.H. Liu, Q. Wang, Y.L. Song, D.W. Zhang, S.R. Yu and X.Y. Zhu, *J. Alloy. Compd*. 473 (2009) 550.
18. C.M. Xu, Y.H. Zhang, G.X. Cheng and W.S.Zhu, *Chinese J. Chem. Eng*. 14 (2006) 829.

19. D. Starosvetsky, O. Khaselev, J. Starosvetsky, R. Armon and J. Yahalom, *Corros. Sci*. 42 (2000) 345.
20. R. J. Zuo, E. Kus, F. Mansfeld and T.K. Wood, *Corros. Sci.* 47 (2005) 279.
21. W. M. Dunne, Jr. *Clin. Microbiol. Rev*. 15 (2002) 155.
22. K.M. Moon, H.R. Cho, M.H. Lee, S.K. Shin and S.C. *Koh, Met. Mater. Int.* 13 (2007) 211.
23. C. N. Cao, Principles of electrochemistry of corrosion (third edition), Chemical industry press, China (2008).
24. W. Lee and W. G. Charachlis, *Corrosion*. 49 (1993) 186.
25 R. Torres-Sanchez, J. Garcia-Vargas, A. Alfonso-Alonso and L. Martinez-Gomez, *Mater. Corros*. 52 (2001) 614.
26. C. Sun, J. Xu, F. H. Wang and C. K. Yu, *Mater. Corros.* 61 (2010) 762.
27. W. P. Iverson, *Nature*. 217 (1968) 1265.
28. W. P. Iverson, *Mater. Performance.* 5 (1998) 46.
29. X.X. Sheng, Y.P. Ting and S.O. Pehkonen, *Corros. Sci.* 49 (2007) 2159.
30. B.C. Syrett, D.D. Macdonald and S.S. Wing, *Corrosion.* 35 (1979) 409.